LANGMUIR

pubs.acs.org/Langmuir Article

Olefin-Bridged Bidentate Adsorbates for Generating Self-Assembled Monolayers on Gold

Siwakorn Sakunkaewkasem, Mario A. Gonzalez, Maria D. Marquez, and T. Randall Lee*

Cite This: *Langmuir* 2020, 36, 10699−10707 Read Online

ACCESS | Metrics & More | Article Recommendations | Supporting Information

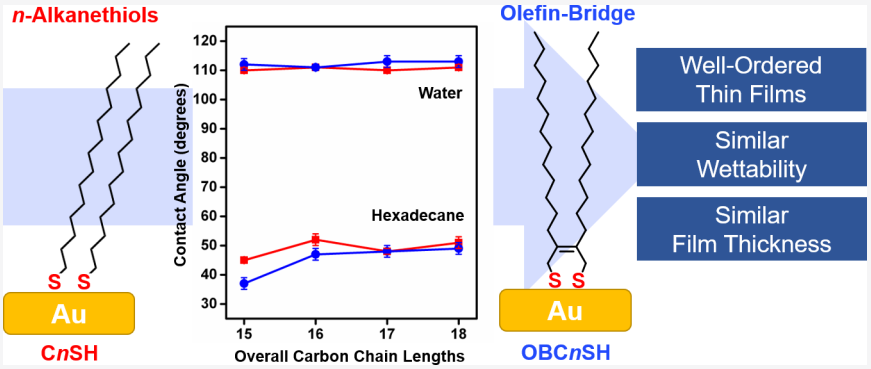

ABSTRACT: A series of custom-designed olefin-bridged bidentate adsorbates composed of an olefin group linking symmetrical hydrocarbon moieties of varying chain lengths was synthesized and used for the preparation of self-assembled monolayers (SAMs) on gold. The structures of the adsorbates are in the form Z-$[CH_3(CH_2)_m]_2(C{=}C)[CH_2SH]_2$ (**OBC*n*SH**) where m = 12−15 and n = m + 3 (**OBC15SH**, **OBC16SH**, **OBC17SH**, and **OBC18SH**). The influence of the olefin linker on the structural and interfacial properties of the SAMs was investigated and compared to SAMs formed from analogous *n*-alkanethiols. Characterization techniques included ellipsometry, X-ray photoelectron spectroscopy (XPS), polarization modulation-infrared reflection−adsorption spectroscopy (PM-IRRAS), and contact angle measurements. The **OBC*n*SH** SAMs exhibited ellipsometric thicknesses that were similar to their monodentate counterparts, suggesting that the new olefin-bridged adsorbates pack similarly to the monodentate analogs. Characterization by PM-IRRAS revealed that the **OBC*n*SH** SAMs were as conformationally ordered as those derived from the reference *n*-alkanethiols with the exception of the adsorbate with the shortest chain length **OBC15SH**, which exhibited low coverage and a liquid-like structure. Unlike the SAMs derived from the *n*-alkanethiols, the **OBC*n*SH** SAMs failed to exhibit "odd−even" effects. However, the **OBC*n*SH** SAMs displayed similar hexadecane contact angles as their *n*-alkanethiol counterparts with the exception of **OBC15SH**, which exhibited markedly diminished hexadecane contact angles. The similar structural and interfacial properties of the **OBC*n*SH** SAMs, when compared to analogous *n*-alkanethiol SAMs, render the molecular architecture of the olefin-bridged dithiol as a robust platform for the synthesis of adsorbates with two chemically distinct tailgroups for use in the preparation and study of phase-incompatible "conflicted" interfaces.

INTRODUCTION

Organic thin films are well-known materials that can be used to modify interfacial properties. The use of self-assembled monolayers (SAMs) is a ubiquitous approach taken by several researchers to manipulate the properties of surfaces for use in a variety of applications, such as anti-adhesive/anti-fouling surfaces for biosensors,[1−3] catalyst modifiers for hydrogenation reactions,[4,5] corrosion protection for metal surfaces,[6,7] lubricants for microelectromechanical systems (MEMs),[8] polymer brushes for biotechnology applications[9] and patterning surfaces,[10,11] and organic thin-film transistors for semiconductors.[12] Much of the research performed on thiolate-based SAMs involve the use of monodentate adsorbates (i.e., adsorbates with one thiol headgroup). However, research has shown that modification of the headgroup architecture to include multiple thiol groups (e.g., bidentate and tridentate adsorbates) leads to enhanced bonding with the metal surface,[13] and subsequently, more stable monolayer films. The enhanced stability of multidentate adsorbates has been attributed to the "chelate effect" where the binding of a multidentate adsorbate is more entropically favorable than that of a monodentate adsorbate.[14] Several types of multidentate

Received: May 8, 2020
Revised: August 3, 2020
Published: August 17, 2020

https://dx.doi.org/10.1021/acs.langmuir.0c01373
Langmuir 2020, 36, 10699−10707

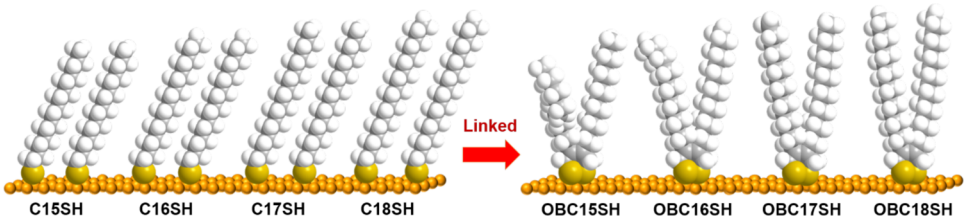

Figure 1. Space-filling models of the investigated SAMs on gold derived from the *n*-alkanethiols (left, **C*n*SH**, *n* = 15−18) and the olefin-bridged dithiols (right, **OBC*n*SH**, *n* = 15−18) with possible gauche defects illustrated for the latter.

adsorbates have been investigated, such as aromatic-based dithiols, spiroalkanedithiols, and several types of trithiol adsorbates.[14,15] Despite the greater stability achieved by multidentate adsorbates, these investigations revealed that multidentate adsorbates, due to their sterically bulky headgroups, produced films with diminished chain density, which can hinder their efficacy as protective barriers toward corrosion or oxidation.[16]

To address the diminished chain density challenge while at the same time exploring the development of new bidentate adsorbates, this study proposes a new class of double-chained, bidentate adsorbate having a headgroup architecture in which the two chains are connected by an olefin linker (see Figure 1). This adsorbate design is attractive due to the sterically small size of the olefin moiety connecting the alkyl chains, which should add little or no steric bulk when compared to two separate *n*-alkanethiol adsorbates. Given these considerations, we envisioned that SAMs derived from olefin-bridged adsorbates would produce films indistinguishable from analogous *n*-alkanethiols. Herein, we designed, synthesized, and characterized a series of symmetrical olefin-bridged dithiols of the form Z-$[CH_3(CH_2)_m]_2(C{=}C)[CH_2SH]_2$ (**OBC*n*SH**) where *m* = 12−15 and *n* = *m* + 3 (**OBC15SH**, **OBC16SH**, **OBC17SH**, and **OBC18SH**). The SAMs derived from the olefin-bridged dithiols on gold were characterized and compared to those generated from a series of analogous monothiol adsorbates having similar chain lengths, **C*n*SH** where *n* = 15−18 (**C15SH**, **C16SH**, **C17SH**, and **C18SH**). We characterized the monolayers by using ellipsometry, X-ray photoelectron spectroscopy (XPS), polarization modulation-infrared reflection−adsorption spectroscopy (PM-IRRAS), and contact angle goniometry.

EXPERIMENTAL SECTION

Descriptions of the materials used in this research, synthetic procedures, spectroscopic characterization of the adsorbates (^{1}H and ^{13}C NMR spectroscopy, as shown in Figures S1−S8), techniques used to analyze the monolayers (ellipsometry, PM-IRRAS, XPS, and contact angle goniometry), additional XPS analyses (Figures S9 and S10 and Tables S1 and S2), and procedures to evaluate film stability are provided in the Supporting Information.

Nomenclature. The nomenclature of the adsorbates and their corresponding abbreviations are pentadecane-1-thiol, **C15SH**; hexadecane-1-thiol, **C16SH**; heptadecane-1-thiol, **C17SH**; octadecane-1-thiol, **C18SH**; (*Z*)-2,3-ditridecylbut-2-ene-1,4-dithiol, **OBC15SH**; (*Z*)-2,3-ditetradecylbut-2-ene-1,4-dithiol, **OBC16SH**; (*Z*)-2,3-dipentadecylbut-2-ene-1,4-dithiol, **OBC17SH**; and (*Z*)-2,3-dihexadecylbut-2-ene-1,4-dithiol, **OBC18SH** (see Figure 1).

RESULTS AND DISCUSSION

Selecting a Solvent for the Formation of the OBC*n*SH SAMs. To determine the optimal conditions for generating covalently bound and well-ordered SAMs from the **OBC*n*SH** adsorbates, **OBC15SH** was chosen as a representative adsorbate to test a variety of developing solvents: ethanol (EtOH), *N*,*N*-dimethylformamide (DMF), isooctane, tetrahydrofuran (THF), and mixtures of THF:EtOH. The SAMs derived from our representative adsorbate in these selected solvents were thoroughly characterized by ellipsometry (to determine thickness), XPS (to determine the chemical composition and nature/environment of the sulfur atom), and PM-IRRAS (to determine the conformational order of the alkyl chains).

Selecting a Solvent Based on Ellipsometric Thickness. The average thickness data collected on the **OBC15SH** SAM after immersion for 48 h in each of the selected solvents are shown in Table 1. The **OBC15SH** SAMs developed in ethanol (EtOH) provided the thickest films at 19 Å, which is also similar to the thickness generated from the analogous *n*-alkanethiol, **C15SH** (18 Å). The **OBC15SH** SAMs developed in DMF, isooctane, and THF exhibited thicknesses of 17, 14, and 10 Å, respectively. The results also indicate that equilibration in THF led to the thinnest films compared to the other solvents. Based on our analysis of the percent of bound sulfur, *vide infra*, for the SAMs developed in EtOH and THF, we also chose to generate **OBC15SH** SAMs in various mixtures of THF and EtOH. Upon increasing the amount of the THF in the mixed solvent systems, a decrease in the film thickness was observed, which agrees with the thickness data obtained in 100% THF. We note also that **OBC15SH** SAMs generated in EtOH, DMF, and minimum amounts of THF (1 and 5%) produced films similar in thickness to those generated from **C15SH**. On the whole, the limited information gained from the thickness measurements is insufficient to select an optimal solvent. We thus sought further analysis of the generation of **OBC15SH** SAMs by using XPS and PM-IRRAS, as described in the following sections.

Table 1. Ellipsometric Thickness of the OBC15SH SAMs Developed in Various Solvents

solvent[a]	thickness (Å)	solvent[a,b]	thickness (Å)
EtOH	19 ± 1	1% THF	18 ± 1
DMF	17 ± 1	5% THF	18 ± 1
isooctane	14 ± 1	10% THF	17 ± 1
THF	10 ± 1	25% THF	16 ± 1

[a]Thickness measurements were taken at rt (23 °C). [b]Several volume % amounts of THF in EtOH were used. SAMs generated from **C15SH** were 18 ± 1 Å. Reported values are the average of at least three separate experiments.

Selecting a Solvent Based on Sulfur Binding Determined by XPS. The **OBC15SH** SAMs generated in each of the developing solvents were analyzed with high-resolution XPS (HR-XPS) in the S 2p region, the spectra shown in Figure 2.

https://dx.doi.org/10.1021/acs.langmuir.0c01373
Langmuir 2020, 36, 10699−10707

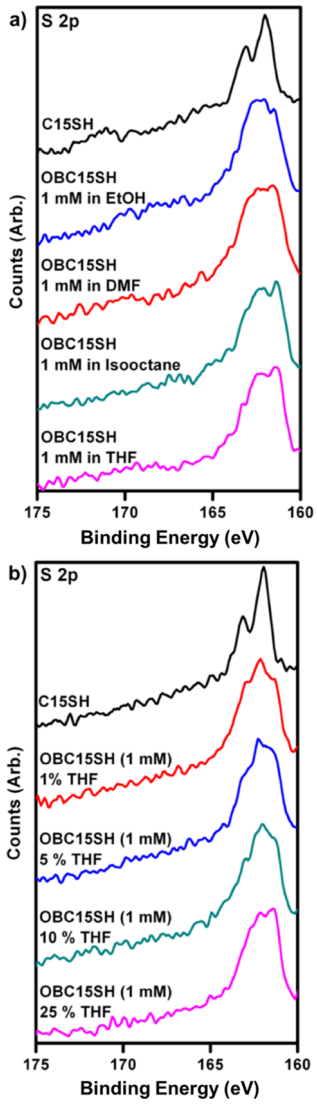

Figure 2. XPS spectra of the S 2p region for SAMs generated from OBC15SH in (a) pure solvents (EtOH, DMF, isooctane, and THF) and (b) various volume % mixtures of THF in EtOH. The SAM generated from C15SH (EtOH) is included in both panels as a reference.

This type of complex spectrum has been observed by San Juan and Carmichael[17] and is indicative of a mixture of sulfur species. To determine the amount of bound sulfur, the S 2p peaks were deconvoluted, presuming a Gaussian/Lorentzian (70:30%) line shape with a splitting energy of 1.18 eV for the S $2p_{3/2}$ and S $2p_{1/2}$ peaks. The deconvolution of all **OBC15SH** SAMs is shown in Figure S9, and the percentages of bound and unbound thiol are presented in Table 2. The spectra demonstrate the presence of bound and unbound sulfur species in all of the conditions tested. The SAMs generated in EtOH produced the greatest amount of bound thiol (87%), while those generated in the THF/EtOH mixture exhibited similar results (81−86%). However, the SAMs generated in DMF, isooctane, and THF exhibited lesser amounts of bound sulfur species. From this analysis, it appears that EtOH and mixtures of EtOH and a minimal amount of THF (1 and 5%) generate monolayers with the greatest degree of S−Au binding.

Selecting a Solvent Based on Conformational Order Determined by PM-IRRAS. To evaluate the conformational order of the SAMs, the **OBC15SH** SAMs equilibrated in various solvents were analyzed using PM-IRRAS. The position of the antisymmetric C−H stretch of the methylene ($\nu_{as}^{CH_2}$) can be used to judge the conformational order of the hydrocarbon chains; for example, a conformationally ordered alkyl chain in the trans-extended conformation exhibits a $\nu_{as}^{CH_2}$ peak at 2918 cm^{-1},[13,18] and deviations to higher wavenumbers indicate the presence of conformationally disordered chains.[6−8,19,20] The PM-IRRAS spectra of the C−H stretching region for the **OBC15SH** SAMs are shown in Figure 3, and the $\nu_{as}^{CH_2}$ peak positions are given in Table 3. SAMs derived from the analogous *n*-alkanethiol, **C15SH**, were used as a reference to compare and contrast the conformational order of the **OBC15SH** SAMs. As shown in Table 3, the **C15SH** SAMs exhibited a $\nu_{as}^{CH_2}$ peak at 2919 cm^{-1}, which is consistent with a conformationally ordered trans-extended chain.[20]

Table 2. Percentage of Bound Sulfur in the OBC15SH SAMs Developed in Various Solvents[a]

solvent	bound sulfur (%)	solvent	bound sulfur (%)
EtOH	87 ± 4	1% THF	85 ± 4
DMF	71 ± 5	5% THF	86 ± 4
isooctane	71 ± 4	10% THF	84 ± 5
THF	77 ± 4	25% THF	81 ± 3

[a]Reported values are the average of at least three separate experiments.

For the **OBC15SH** SAMs, there is a degree of disorder in all of the SAMs regardless of the solvent used. However, only the SAMs generated in EtOH, or a mixture containing EtOH, produced SAMs with greater conformational order than those generated in DMF, isooctane, or pure THF. For the single-component solvents, the conformational order of the chains decreased in the following order: ethanol ≫ DMF > THF ∼ isooctane. In the THF:EtOH mixtures, the $\nu_{as}^{CH_2}$ peak position of the **OBC15SH** SAMs increased with increasing amounts of THF: 2922 (1% THF) to 2925 cm^{-1} (25% THF). Apparent from the data, higher amounts of THF in the solvent have a detrimental effect on the conformational order of the chains due to diminished molecular packing densities and consequently weaker interchain van der Waals interactions in the films (Table S1 lists the packing densities).

Considering all the data collected, the optimal solvent for the development of the **OBC*n*SH** SAMs is EtOH. The **OBC15S1H** SAMs generated in EtOH produced films with similar thicknesses as those derived from the **C15SH** analog. Furthermore, the **OBC15SH** SAMs generated in EtOH exhibited the greatest percentage of bound sulfur and the most conformationally ordered chains. Thus, our analysis of **OBC*n*SH** SAMs in this study utilized films that were developed in EtOH.

Characterization of the OBC*n*SH SAMs Developed in Ethanol. *Ellipsometric Thicknesses of the OBCnSH SAMs.* We chose an equilibration time of 48 h for developing the **OBC*n*SH** SAMs based on the equilibration time used for similarly structured bidentate adsorbates reported in the literature.[21,22] The thicknesses of the **OBC*n*SH** SAMs and the analogous *n*-alkanethiol SAMs (derived from **C*n*SH**) are shown in Table 4. SAMs derived from **C*n*SH** were used as reference films for the direct comparison of the surface properties with the new **OBC*n*SH** SAMs. For the **C*n*SH** SAMs, the thickness measurements are within the experimental error of the literature values: 17, 18, 20, and 21 Å for the

https://dx.doi.org/10.1021/acs.langmuir.0c01373
Langmuir 2020, 36, 10699−10707

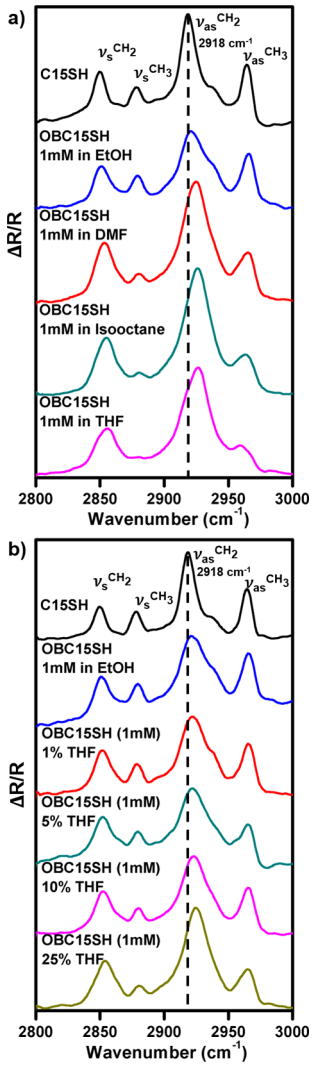

Figure 3. PM-IRRAS spectra of the C−H stretching region for the **OBC15SH** SAMs generated in (a) pure solvents (EtOH, DMF, isooctane, and THF) and (b) various volume % mixtures of THF in EtOH. The SAM generated from **C15SH** (EtOH) are included in both panels as a reference.

Table 3. Position of the $\nu_{as}^{CH_2}$ Peak for the OBC15SH SAMs Developed in Various Solvents[a]

solvent	$\nu_{as}^{CH_2}$ (cm^{-1})	solvent	$\nu_{as}^{CH_2}$ (cm^{-1})
EtOH	2921	1% THF	2922
DMF	2925	5% THF	2922
isooctane	2926	10% THF	2923
THF	2926	25% THF	2925

[a]SAMs generated from **C15SH** exhibited a $\nu_{as}^{CH_2}$ at 2919 cm^{-1}. Reported values are the average of at least three separate experiments.

C15SH, **C16SH**, **C17SH**, and **C18SH** SAMs, respectively.[23] The **OBC*n*SH** SAMs produced films with correspondingly similar film thicknesses: 17, 20, 21, and 22 Å for the **OBC15SH**, **OBC16SH**, **OBC17SH**, and **OBC18SH** SAMs, respectively. The similarities in the thickness data for the two sets of SAMs suggest similar packing and/or chain orientation (i.e., tilt angle) for the **OBC*n*SH** SAMs and the **C*n*SH** SAMs.

*Conformational Order of the **OBCnSH** SAMs.* Insight into the conformational order of the alkyl chains in the SAMs was obtained by evaluating the C−H stretching region of the

Table 4. Ellipsometric Thickness for the *n*-Alkanethiols and Olefin-Bridged Dithiol SAMs[a]

adsorbate	thickness (Å)	adsorbate	thickness (Å)
C15SH	17 ± 1 (18)	**OBC15SH**	17 ± 1
C16SH	18 ± 1 (20)	**OBC16SH**	20 ± 1
C17SH	20 ± 1 (21)	**OBC17SH**	21 ± 1
C18SH	21 ± 1 (22)	**OBC18SH**	22 ± 1

[a]The reference values for the **C*n*SH** SAMs are presented in parentheses. Reported values are the average of at least three separate experiments.

monolayers by surface infrared spectroscopy (specifically PM-IRRAS). In our evaluation, we used the position of the antisymmetric C−H stretching of the methylene groups ($\nu_{as}^{CH_2}$) to estimate the conformational order/crystallinity of the SAMs.[19,24,25] The PM-IRRAS spectra of the C−H stretching region of the **C*n*SH** and **OBC*n*SH** SAMs are shown in Figure 4, and the peak positions and assignments are provided in Table 5.

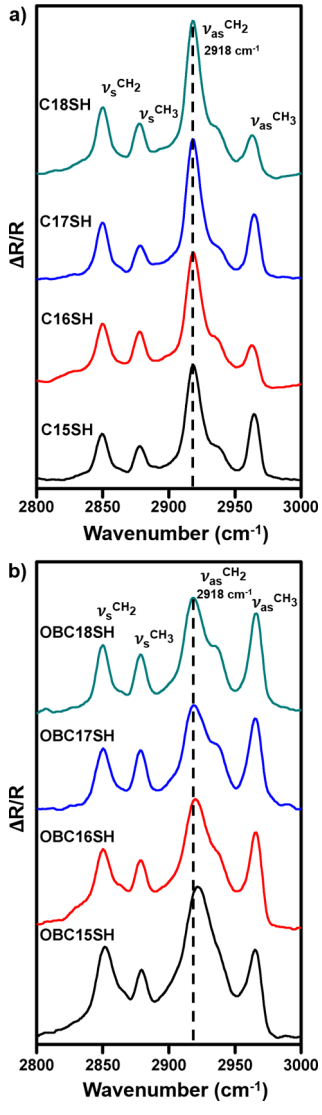

Figure 4. PM-IRRAS spectra of the C−H stretching region for (a) the **C*n*SH** SAMs and (b) the **OBC*n*SH** SAMs.

https://dx.doi.org/10.1021/acs.langmuir.0c01373
Langmuir 2020, 36, 10699−10707

Table 5. PM-IRRAS Data for the SAMs Generated from the C*n*SH and OBC*n*SH Adsorbates[a]

adsorbate	$\nu_s^{CH_2}$ (cm^{-1})	$\nu_s^{CH_3}$ (cm^{-1})	$\nu_{as}^{CH_2}$ (cm^{-1})	$\nu_{as}^{CH_3}$ (cm^{-1})
C15SH	2849	2878	2919	2964
C16SH	2849	2878	2918	2963
C17SH	2849	2877	2918	2964
C18SH	2849	2877	2918	2963
OBC15SH	2851	2879	2921	2966
OBC16SH	2850	2878	2920	2966
OBC17SH	2850	2878	2919	2965
OBC18SH	2850	2878	2918	2965

[a]Reported values are the average of at least three separate experiments.

All **C*n*SH** SAMs exhibit a $\nu_{as}^{CH_2}$ band at 2918 cm^{-1}, indicating well-ordered alkyl chains that are mostly in the trans-extended conformation.[19,20] However, for the **OBC*n*SH** SAMs, only the longer chained adsorbates, **OBC17SH** and **OBC18SH**, produced SAMs with a $\nu_{as}^{CH_2}$ band at 2918 cm^{-1}. The shorter chained adsorbates, **OBC15SH** and **OBC16SH**, produced SAMs with a $\nu_{as}^{CH_2}$ band at higher wavenumbers, 2921 and 2920 cm^{-1}, respectively, indicating a slight disorder in the alkyl chains.[26] As commonly observed with SAMs on gold derived from *n*-alkanethiols,[19,20,27] the conformational order of the **OBC*n*SH** SAMs was observed to increase as the length of the carbon chain was extended; moreover, the IR data suggest that a minimum of 16 methylene units are required to produce highly ordered films from the **OBC*n*SH** adsorbates. In contrast, research has shown that *n*-alkanethiol SAMs require as few as 10 methylene units to generate well-ordered SAMs.[19,20,27]

The need to have longer methylene units for conformationally ordered **OBC*n*SH** SAMs compared to **C*n*SH** SAMs can be attributed to the headgroup architecture of the adsorbate. In the **OBC*n*SH** SAMs, the planar olefin moiety that connects both alkyl chains together hinders the alkyl chains from easily maximizing interchain van der Waals interactions. In addition, the bond-angle constraints and rigidity of the olefinic moiety in these adsorbates can plausibly lead to an effective increase in steric bulk and play a role in the need for longer methylene chains to induce intermolecular order. In contrast, *n*-alkanethiol SAMs are less structurally constrained. To compensate for structural constraints in the **OBC*n*SH** SAMs, longer alkyl chains are required to achieve maximum van der Waals interactions and high conformational order.

We note also that the PM-IRRAS data support a parity or "odd−even" effect in the **C*n*SH** SAMs and an absence of one in the **OBC*n*SH** SAMs. Specifically, the relative intensities of the asymmetric and symmetric CH_3 stretching bands alternate between odd and even chain lengths only for the **C*n*SH** SAMs. Specifically, for the odd chain lengths (**C15SH** and **C17SH**), the asymmetric band is greater in intensity than the symmetric band; conversely, for the even chain lengths (**C16SH** and **C18SH**), the intensity of the bands is roughly the same. This phenomenon arises due to the systematically varying orientation of the terminal methyl groups as a function of chain length.[28] In contrast, the relative intensities of the asymmetric and symmetric CH_3 stretching bands in the **OBC*n*SH** SAMs are invariant with the chain length, indicating no systematic variation in the methyl group orientation for the **OBC*n*SH** SAMs (i.e., no odd−even effect; *vide infra*).

*Analysis of the **OBCnSH** SAMs by XPS.* X-ray photoelectron spectroscopy (XPS) is a powerful method used to identify the elemental composition of surfaces.[29] Elemental identification can be achieved by evaluating the binding energies (BEs) of the emitted photoelectrons, which are affected by the chemical and electronic environment (i.e., oxidation state) of individual atoms.[30] Two areas of interest for the SAMs analyzed herein are the sulfur and carbon regions. The XPS spectra for the S 2p and C 1s regions of the **C*n*SH** and **OBC*n*SH** SAMs are shown in Figure 5.

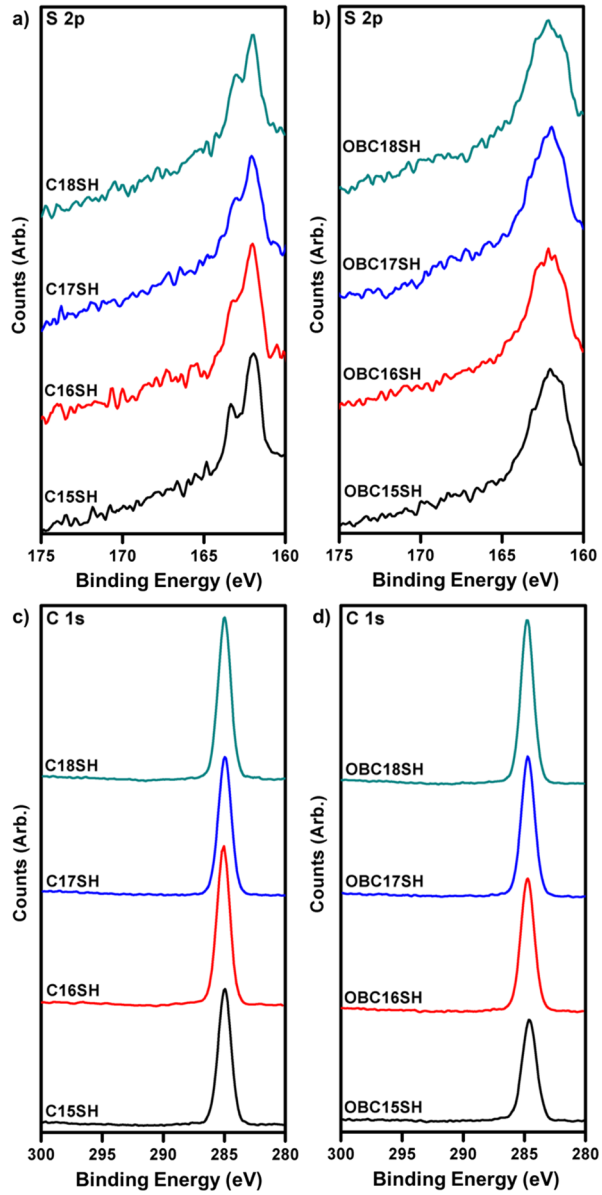

Figure 5. XPS spectra of the (a, b) S 2p and (c, d) C 1s regions for the **C*n*SH** and **OBC*n*SH** SAMs.

The nature of the Au−S bond can be determined by analysis with XPS with particular focus on the BEs of the sulfur species in the S 2p region.[29] The differences in the chemical and electronic environments of the sulfur atoms will lead to distinguishable peaks in the spectra that reveal whether the sulfur is covalently bound to the surface of gold, unbound, and/or oxidized. For bound thiols, the S 2p peak appears as a

https://dx.doi.org/10.1021/acs.langmuir.0c01373
Langmuir 2020, 36, 10699−10707

doublet, S $2p_{3/2}$ and S $2p_{1/2}$, in a 2:1 ratio with the S $2p_{3/2}$ at a BE of ∼162 eV.[29] The BE of the S $2p_{3/2}$ peak of unbound thiols appears at ∼163 eV while that for oxidized sulfur species appears at 167−169 eV.[29,31] This information can be used to assess the bonding behavior of the adsorbate on the surface.[29] The S 2p spectra of the **C*n*SH** SAMs exhibit mostly bound thiols, S $2p_{3/2}$ peak at ∼162 eV; furthermore, there is no evidence of highly oxidized sulfur species in the samples. However, as noted above for the **OBC15SH** SAM, the spectra of all of the **OBC*n*SH** SAMs exhibit a complex peak in the S 2p region. To determine the amount of bound sulfur in the **OBC*n*SH** SAMs, the S 2p peaks were deconvoluted according to the procedure described in the Supporting Information (see Figure S10). The percentage of bound thiol for the **OBC*n*SH** SAMs is listed in Table 6 and are 87, 85, 88, and 87% for **OBC15SH**, **OBC16SH**, **OBC17SH**, and **OBC18SH**, respectively.

Table 6. Percentage of Bound Sulfur, Binding Energy, and Relative Packing Density of the OBC*n*SH SAMs[a]

adsorbate	bound sulfur (%)	C 1s (eV)	relative packing density
OBC15SH	87 ± 4	284.6	0.80 ± 0.03
OBC16SH	85 ± 3	284.8	0.90 ± 0.01
OBC17SH	88 ± 4	284.8	0.92 ± 0.02
OBC18SH	87 ± 4	284.9	0.92 ± 0.03

[a]To determine the relative packing density, the C/Au ratios of the analogous **C*n*SH** SAMs were calculated and normalized to be 1.00. Reported values are the average of at least three separate experiments.

In addition to obtaining the elemental composition of a monolayer by XPS, a qualitative analysis of the chain density can be obtained. The C 1s spectra of the **C*n*SH** and **OBC*n*SH** SAMs exhibit only one peak characteristic of the CH_2/CH_3 units. The BE of this peak, as listed in Table 6 for each of the **OBC*n*SH** SAMs, can be used to gain insight into the packing density of the chains. Using the **C*n*SH** SAMs as standards for densely packed SAMs (i.e., 100% packing), the chain packing density of the **OBC*n*SH** SAMs can be obtained. For the **C*n*SH** SAMs, the BE of this peak for all adsorbates in the series appeared at 285.0 eV, consistent with previous reports.[23,32] For the **OBC*n*SH** SAMs, the BE of the C 1s peak appeared at a slightly lower value than that for the **C*n*SH** SAMs. Upon increasing the carbon chain length in the series, an increase in the BE was observed: 284.6, 284.8, 284.8, and 284.9 eV for the **OBC15SH**, **OBC16SH**, **OBC17SH**, and **OBC18SH** SAMs, respectively. The shift to a lower binding energy, compared to the **C*n*SH** SAMs, in the **OBC*n*SH** SAMs is consistent with films having lower chain packing densities (i.e., loosely packed films). Loosely packed films act as inefficient insulators, easily ejecting the photoelectrons compared to densely packed films. Consequently, the positive charge generated during the process can be readily discharged, which leads to diminished binding energies.[26,33−35]

For a more quantitative analysis of the **OBC*n*SH** SAMs, the relative packing densities of the films are provided in Table 6, which are determined from the C/Au ratios (derived from the atomic percentages of the respective elements) shown in Table S2. Apparent from the values listed in Table 6, as the carbon length was increased in the **OBC*n*SH** series, the relative packing density also increased, in agreement with the shifts in the BE of the C 1s peak (vide supra). Interesting to note is the correlation between the relatively lower packing density of the **OBC15SH** SAM, 0.80 ± 0.01, and the enhanced conformational disorder in this indicated by the PM-IRRAS spectra. Evident from the XPS and PM-IRRAS data, the longer carbon chains enable the alkyl chains to pack more densely. This type of correlation has been well established in studies of SAMs generated from *n*-alkanethiols.[20]

*Wettability Studies of the **OBCnSH** SAMs.* The advancing contact angle of polar and nonpolar liquids can be used to evaluate the interfacial properties of the tested surface.[36−38] Particularly, the contact angles of hexadecane can give useful information regarding the structural features of hydrocarbon-based films.[23,39] Consequently, in the present study, we used both water and hexadecane as probe liquids to evaluate all of the SAMs derived from the **C*n*SH** and **OBC*n*SH** adsorbates. All of the collected contact angle data (advancing and receding) are shown in Table 7; furthermore, Figures 6 and 7 show optical images of the advancing contact angles with water and hexadecane, respectively, as contacting liquids.

Table 7. Advancing Contact Angles (°) and Hysteresis Values ($\Delta\theta = \theta_a - \theta_r$, °) of the C*n*SH and OBC*n*SH SAMs[a]

adsorbates	water	hexadecane (HD)
C15SH	110 ± 1 (4)	45 ± 1 (3)
C16SH	111 ± 1 (6)	52 ± 2 (5)
C17SH	110 ± 1 (6)	48 ± 1 (4)
C18SH	111 ± 1 (7)	51 ± 2 (5)
OBC15SH	112 ± 2 (4)	37 ± 2 (4)
OBC16SH	111 ± 1 (5)	47 ± 2 (4)
OBC17SH	113 ± 2 (7)	48 ± 2 (5)
OBC18SH	113 ± 2 (7)	49 ± 2 (6)

[a]Reported values are the average of at least nine measurements.

As shown in Table 7 and Figure 6, the advancing contact angles of water on the **C*n*SH** SAMs remained relatively constant at 110°, regardless of the number of carbons in the chain. Similarly, the contact angles of water on the **OBC*n*SH** SAMs also remained constant throughout the series at ∼111 ± 1°. Moreover, both types of SAMs exhibit the same degree of hydrophobicity.

The contact angles of hexadecane on the **C*n*SH** SAMs exhibited values of 45 ± 1, 52 ± 2, 48 ± 1, and 51 ± 2° for the SAMs derived from **C15SH**, **C16SH**, **C17SH**, and **C18SH**, respectively, as shown in Figure 7. Interesting to note is the trend in the wettability data of the **C*n*SH** SAMs. The SAMs with an even number of carbons in the chain, **C16SH** and **C18SH**, gave higher contact angles than the odd-numbered chains, **C15SH** and **C17SH**. This parity effect, or odd−even effect, has been observed in several SAMs in the literature and has been attributed to the orientation of the terminal group in the hydrocarbon chain.[40−43] In the **OBC*n*SH** SAMs, the contact angles of hexadecane on **OBC15SH**, **OBC16SH**, **OBC17SH**, and **OBC18SH** were 37 ± 2, 47 ± 2, 48 ± 2, and 49 ± 2°, respectively, as shown in Figure 7. In contrast to the normal alkanethiols, there was no odd−even effect[43] for the **OBC*n*SH** series; rather, a steadily increasing contact angle was observed (i.e., decreasing wettability) as the chain length was systematically increased. The absence of an odd−even effect can plausibly arise from various factors such as (i) random orientations of the terminal groups in the **OBC*n*SH** SAMs and (ii) different tilt and twist angles in the **OBC*n*SH** SAMs compared to the **C*n*SH** SAMs. Both of these rationalizations can be attributed to the structurally constrained olefinic

https://dx.doi.org/10.1021/acs.langmuir.0c01373
Langmuir 2020, 36, 10699−10707

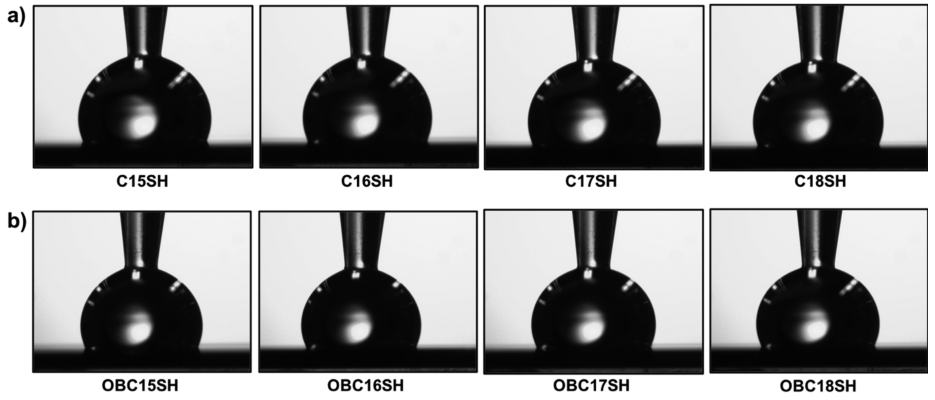

Figure 6. Optical images of the advancing contact angles of water on (a) the **C*n*SH** SAMs and (b) the **OBC*n*SH** SAMs.

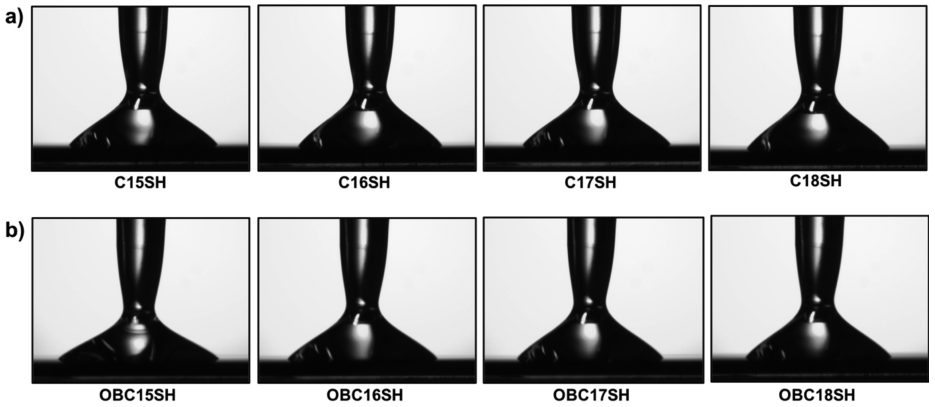

Figure 7. Optical images of the advancing contact angles of hexadecane on (a) the **C*n*SH** SAMs and (b) the **OBC*n*SH** SAMs.

bridges in the headgroup of the **OBC*n*SH** adsorbates. Regardless, the contact angle data of the new SAMs suggest that the adsorbates with long carbon chains can generate higher contact angles of hexadecane (i.e., less wettable films) than those with shorter carbon chains, corroborating the conclusions made with the other surface techniques used in this study (ellipsometry, PM-IRRAS, and XPS).

The contact angle data collected can be further analyzed to give insight into the heterogeneity, or roughness, of the interfaces of the films. In particular, the hysteresis values can be obtained by taking the difference between the advancing and receding contact angles (i.e., $\Delta\theta = \theta_a - \theta_r$). Table 7 shows the hysteresis data for the **C*n*SH** and **OBC*n*SH** SAMs (see values in parentheses). For the **C*n*SH** SAMs, the hysteresis values are consistent with literature reports (3−7°).[44] The SAMs generated from the **OBC*n*SH** adsorbates have hysteresis values that fall within those obtained from the corresponding **C*n*SH** SAM (4−7°). The similar hysteresis values of the **OBC*n*SH** SAMs and the **C*n*SH** SAMs indicate that the interfaces generated from the **OBC*n*SH** adsorbates have similar roughness/heterogeneity as those generated from the **C*n*SH** adsorbates.

Preliminary Studies of Film Stability. Using ellipsometric thickness measurements, we briefly evaluated the stabilities of the SAMs derived from the olefin-bridged dithiols (**OBC*n*SH**) and compared the results to those obtained from the SAM derived from **C18SH**. For SAMs exposed continuously to ambient air and soft light, the ellipsometry data in Figure S11a show that the **OBC*n*SH** SAMs underwent desorption over a period of 5 days with the **OBC18SH** SAM being the most stable in the series with ∼80% of the SAM remaining on the substrate. Correspondingly, the **OBC*n*SH** SAM having the shortest chain length (**OBC15SH**) desorbed most readily (∼70% remaining on the surface). Importantly, all of the **OBC*n*SH** SAMs degraded more readily than the **C18SH** SAM. We also examined the desorption profiles of the SAMs at an elevated temperature of 80 °C in isooctane (see Figure S11b). Substantial desorption of the **OBC*n*SH** SAMs was observed with ∼20% of the SAMs remaining on the surface after 1 h of exposure compared to ∼80% for the **C18SH** SAM.

When compared to other SAMs generated from bidentate adsorbates in the literature,[14] the characterization data in the preceding sections show that the **OBC*n*sH** SAMs more closely resemble *n*-alkanethiol SAMs (**C*n*SH**) in terms of structural features, including packing density and conformational order. Nevertheless, the **OBC*n*SH** SAMS appear to be markedly less stable than those generated from other bidentate analogs as well as those generated from **C18SH**. It is possible that the instability of the **OBC*n*SH** SAMS arises from the facile desorption of these molecules from the surface as five-membered ring intramolecular disulfides.[45]

■ CONCLUSIONS

In summary, SAMs generated from the new olefin-bridged dithiols (**OBC*n*SH**, n = 15−18) were prepared and studied. The SAMs were characterized using ellipsometry, PM-IRRAS, XPS, and contact angle measurements. The data obtained were compared to those obtained on SAMs generated from an analogous series of *n*-alkanethiols (**C*n*SH**, n = 15−18). An initial series of experiments found ethanol to be the optimal

https://dx.doi.org/10.1021/acs.langmuir.0c01373
Langmuir 2020, 36, 10699−10707

solvent for monolayer formation from the **OBC*n*SH** adsorbates. While the ellipsometric studies confirmed that the **OBC*n*SH** adsorbates generate monolayer films on gold, analysis by XPS revealed that SAMs derived from these new adsorbates have chain packing densities that are comparable to those of *n*-alkanethiol SAMs. Moreover, the XPS studies showed an increasing chain packing density for the **OBC*n*SH** SAMs as the length of the carbon chains in the adsorbates was increased. Analysis by PM-IRRAS showed that the **OBC*n*SH** SAMs with longer chain lengths (i.e., those derived from **OBC17SH** and **OBC18SH**) have similar conformational order as their analogous **C*n*SH** SAMs, **C17SH** and **C18SH**. Furthermore, the **OBC*n*SH** SAMs have similar hydrophobicity and oleophilicity as the **C*n*SH** SAMs, save for the SAM derived from **OBC15SH**, whose shorter chain length and thus weaker interchain van der Waals stabilization led to SAMs with slightly diminished conformational order. Thus, SAMs generated from the **OBC*n*SH** adsorbates can serve as a new model of bidentate adsorbates that have structural features similar to those of *n*-alkanethiol SAMs in terms of thickness, packing density, and conformational order. Preliminary stability studies revealed that the **OBC*n*SH** SAMs were more prone to decomposition than the **C18SH** SAM, which could plausibly be attributed to the ease of desorption of the **OBC*n*SH** adsorbates as intramolecular disulfides. We envision that unsymmetrical versions of the olefin-bridged dithiols where the chemical composition of the two tailgroups are different will open new avenues for the generation of mixed phase-incompatible interfaces.

■ ASSOCIATED CONTENT

Supporting Information

The Supporting Information is available free of charge at https://pubs.acs.org/doi/10.1021/acs.langmuir.0c01373.

Materials, methods, synthetic procedures, and characterization data (^{1}H and ^{13}C NMR spectra; mass spectrometry) for **OBC15SH**, **OBC16SH**, **OBC17SH**, and **OBC18SH**, additional XPS spectra, and analyses for deconvoluting the S 2p region and calculating the packing densities of the SAMs (PDF)

■ AUTHOR INFORMATION

Corresponding Author

T. Randall Lee − *Department of Chemistry and the Texas Center for Superconductivity, University of Houston, Houston, Texas 77204-5003, United States;* orcid.org/0000-0001-9584-8861; Email: trlee@uh.edu

Authors

Siwakorn Sakunkaewkasem − *Department of Chemistry and the Texas Center for Superconductivity, University of Houston, Houston, Texas 77204-5003, United States*

Mario A. Gonzalez − *Department of Chemistry and the Texas Center for Superconductivity, University of Houston, Houston, Texas 77204-5003, United States*

Maria D. Marquez − *Department of Chemistry and the Texas Center for Superconductivity, University of Houston, Houston, Texas 77204-5003, United States*

Complete contact information is available at: https://pubs.acs.org/10.1021/acs.langmuir.0c01373

Notes

The authors declare no competing financial interest.

■ ACKNOWLEDGMENTS

The National Science Foundation (CHE-1710561, to T.R.L.), the Robert A. Welch Foundation (grant no. E-1320, to T.R.L), and the Texas Center for Superconductivity at the University of Houston (to T.R.L.) provided generous financial support for this research.

■ REFERENCES

(1) Jamison, A. C.; Chinwangso, P.; Lee, T. R. Self-Assembled Monolayers: the Development of Functional Nanoscale Films. *Funct. Polym. Films* **2011**, 151−217.

(2) Krishnan, S.; Weinman, C. J.; Ober, C. K. Advances in polymers for anti-biofouling surfaces. *J. Mater. Chem.* **2008**, *18*, 3405−3413.

(3) Li, Y.; Giesbers, M.; Gerth, M.; Zuilhof, H. Generic Top-Functionalization of Patterned Antifouling Zwitterionic Polymers on Indium Tin Oxide. *Langmuir* **2012**, *28*, 12509−12517.

(4) Kahsar, K. R.; Schwartz, D. K.; Medlin, J. W. Control of Metal Catalyst Selectivity through Specific Noncovalent Molecular Interactions. *J. Am. Chem. Soc.* **2014**, *136*, 520−526.

(5) Pang, S. H.; Schoenbaum, C. A.; Schwartz, D. K.; Medlin, J. W. Effects of Thiol Modifiers on the Kinetics of Furfural Hydrogenation over Pd Catalysts. *ACS Catal.* **2014**, *4*, 3123−3131.

(6) Laibinis, P. E.; Whitesides, G. M. Self-Assembled Monolayers of N-Alkanethiolates on Copper are Barrier Films that Protect the Metal Against Oxidation by Air. *J. Am. Chem. Soc.* **1992**, *114*, 9022−9028.

(7) Patois, T.; Et Taouil, A.; Lallemand, F.; Carpentier, L.; Roizard, X.; Hihn, J.-Y.; Bondeau-Patissier, V.; Mekhalif, Z. Microtribological and Corrosion Behaviors of 1H,1H,2H,2H-Perfluorodecanethiol Self-Assembled Films on Copper Surfaces. *Surf. Coat. Technol.* **2010**, *205*, 2511−2517.

(8) Srinivasan, U.; Houston, M. R.; Howe, R. T.; Maboudian, R. Alkyltrichlorosilane-Based Self-Assembled Monolayer Films for Stiction Reduction in Silicon Micromachines. *J. Microelectromech. Syst.* **1998**, *7*, 252−260.

(9) Senaratne, W.; Andruzzi, L.; Ober, C. K. Self-Assembled Monolayers and Polymer Brushes in Biotechnology: Current Applications and Future Perspectives. *Biomacromolecules* **2005**, *6*, 2427−2448.

(10) Kagan, C. R.; Carmichael, T. B.; Kosbar, L. L. U.S. Patent 7,491,286, 2009.

(11) Slaughter, L. S.; Cheung, K. M.; Kaappa, S.; Cao, H. H.; Yang, Q.; Young, T. D.; Serino, A. C.; Malola, S.; Olson, J. M.; Link, S.; Häkkinen, H.; Andrews, A. M.; Weiss, P. S. Patterning of supported gold monolayers via chemical lift-off lithography. *Beilstein J. Nanotechnol.* **2017**, *8*, 2648−2661.

(12) McDermott, J. E.; McDowell, M.; Hill, I. G.; Hwang, J.; Kahn, A.; Bernasek, S. L.; Schwartz, J. Organophosphonate Self-Assembled Monolayers for Gate Dielectric Surface Modification of Pentacene-Based Organic Thin-Film Transistors: A Comparative Study. *J. Phys. Chem. A* **2007**, *111*, 12333−12338.

(13) Lee, H. J.; Jamison, A. C.; Lee, T. R. Boc-Protected ω-Amino Alkanedithiols Provide Chemically and Thermally Stable Amine-Terminated Monolayers on Gold. *Langmuir* **2015**, *31*, 2136−2146.

(14) Chinwangso, P.; Jamison, A. C.; Lee, T. R. Multidentate Adsorbates for Self-Assembled Monolayer Films. *Acc. Chem. Res.* **2011**, *44*, 511−519.

(15) Marquez, M. D.; Zenasni, O.; Jamison, A. C.; Lee, T. R. Homogeneously Mixed Monolayers: Emergence of Compositionally Conflicted Interfaces. *Langmuir* **2017**, *33*, 8839−8855.

(16) Ulman, A. Formation and Structure of Self-Assembled Monolayers. *Chem. Rev.* **1996**, *96*, 1533−1554.

(17) San Juan, R. R.; Carmichael, T. B. Formation of Self-Assembled Monolayers with Homogeneously Mixed, Loosely Packed Alkyl Groups Using Unsymmetrical Dialkyldithiophosphinic Acids. *Langmuir* **2012**, *28*, 17701−17708.

(18) Sui, W.; Zhao, W.; Zhang, X.; Peng, S.; Zeng, Z.; Xue, Q. Comparative Anti-Corrosion Properties of Alkylthiols SAMs and Mercapto Functional Silica Sol−Gel Coatings on Copper Surface in Sodium Chloride Solution. *J. Solgel. Sci. Technol.* **2016**, *80*, 567−578.
(19) Snyder, R. G.; Hsu, S. L.; Krimm, S. Vibrational Spectra in the C-H Stretching Region and the Structure of the Polymethylene Chain. *Spectrochim. Acta A.* **1978**, *34*, 395−406.
(20) Porter, M. D.; Bright, T. B.; Allara, D. L.; Chidsey, C. E. D. Spontaneously Organized Molecular Assemblies. 4. Structural Characterization of *n*-Alkyl Thiol Monolayers on Gold by Optical Ellipsometry, Infrared Spectroscopy, and Electrochemistry. *J. Am. Chem. Soc.* **1987**, *109*, 3559−3568.
(21) Chinwangso, P.; Lee, H. J.; Lee, T. R. Self-Assembled Monolayers Generated from Unsymmetrical Partially Fluorinated Spiroalkanedithiols. *Langmuir* **2015**, *31*, 13341−13349.
(22) Shon, Y.-S.; Lee, T. R. Chelating Self-Assembled Monolayers on Gold Generated from Spiroalkanedithiols. *Langmuir* **1999**, *15*, 1136−1140.
(23) Bain, C. D.; Troughton, E. B.; Tao, Y. T.; Evall, J.; Whitesides, G. M.; Nuzzo, R. G. Formation of Monolayer Films by the Spontaneous Assembly of Organic Thiols from Solution onto Gold. *J. Am. Chem. Soc.* **1989**, *111*, 321−335.
(24) MacPhail, R. A.; Strauss, H. L.; Snyder, R. G.; Elliger, C. A. Carbon-Hydrogen Stretching Modes and the Structure of *n*-Alkyl Chains. 2. Long, All-Trans Chains. *J. Phys. Chem.* **1984**, *88*, 334−341.
(25) Snyder, R. G.; Strauss, H. L.; Elliger, C. A. Carbon-Hydrogen Stretching Modes and the Structure of N-Alkyl Chains. 1. Long, Disordered Chains. *J. Phys. Chem.* **1982**, *86*, 5145−5150.
(26) Park, J.-S.; Smith, A. C.; Lee, T. R. Loosely Packed Self-Assembled Monolayers on Gold Generated from 2-Alkyl-2-methyl-propane-1,3-dithiols. *Langmuir* **2004**, *20*, 5829−5836.
(27) Ulman, A. *An introduction to ultrathin organic films : from Langmuir-Blodgett to self-assembly*; Academic Press: San Diego, 1991.
(28) Tao, Y.-T. Structural Comparison of Self-Assembled Monolayers of *n*-Alkanoic Acids on the Surfaces of Silver, Copper, and Aluminum. *J. Am. Chem. Soc.* **1993**, *115*, 4350−4358.
(29) Castner, D. G.; Hinds, K.; Grainger, D. W. X-ray Photoelectron Spectroscopy Sulfur 2p Study of Organic Thiol and Disulfide Binding Interactions with Gold Surfaces. *Langmuir* **1996**, *12*, 5083−5086.
(30) Vickerman, J. C. *Surface analysis : the principal techniques*; John Wiley: Chichester [England]: New York, 1997.
(31) Ishida, T.; Choi, N.; Mizutani, W.; Tokumoto, H.; Kojima, I.; Azehara, H.; Hokari, H.; Akiba, U.; Fujihira, M. High-Resolution X-ray Photoelectron Spectra of Organosulfur Monolayers on Au(111): S(2p) Spectral Dependence on Molecular Species. *Langmuir* **1999**, *15*, 6799−6806.
(32) Biebuyck, H. A.; Bain, C. D.; Whitesides, G. M. Comparison of Organic Monolayers on Polycrystalline Gold Spontaneously Assembled from Solutions Containing Dialkyl Disulfides or Alkanethiols. *Langmuir* **1994**, *10*, 1825−1831.
(33) Frey, S.; Heister, K.; Zharnikov, M.; Grunze, M.; Tamada, K.; Colorado, R., Jr.; Graupe, M.; Shmakova, O. E.; Lee, T. R. Structure of Self-Assembled Monolayers of Semifluorinated Alkanethiols on Gold and Silver Substrates. *Isr. J. Chem.* **2010**, *40*, 81−97.
(34) Ishida, T.; Hara, M.; Kojima, I.; Tsuneda, S.; Nishida, N.; Sasabe, H.; Knoll, W. High Resolution X-ray Photoelectron Spectroscopy Measurements of Octadecanethiol Self-Assembled Monolayers on Au(111). *Langmuir* **1998**, *14*, 2092−2096.
(35) Tamada, K.; Ishida, T.; Knoll, W.; Fukushima, H.; Colorado, R.; Graupe, M.; Shmakova, O. E.; Lee, T. R. Molecular Packing of Semifluorinated Alkanethiol Self-Assembled Monolayers on Gold: Influence of Alkyl Spacer Length. *Langmuir* **2001**, *17*, 1913−1921.
(36) Bain, C. D.; Whitesides, G. M. Formation of Monolayers by the Coadsorption of Thiols on Gold: Variation in the Length of the Alkyl Chain. *J. Am. Chem. Soc.* **1989**, *111*, 7164−7175.
(37) Fowkes, F. M.; Riddle, F. L., Jr.; Pastore, W. E.; Weber, A. A. Interfacial Interactions between Self-Associated Polar Liquids and Squalane used to Test Equations for Solid—Liquid Interfacial Interactions. *Colloids Surf.* **1990**, *43*, 367−387.
(38) van Oss, C. J.; Chaudhury, M. K.; Good, R. J. Monopolar Surfaces. *Adv. Colloid Interface Sci.* **1987**, *28*, 35−64.
(39) Nuzzo, R. G.; Dubois, L. H.; Allara, D. L. Fundamental studies of microscopic wetting on organic surfaces. 1. Formation and structural characterization of a self-consistent series of polyfunctional organic monolayers. *J. Am. Chem. Soc.* **1990**, *112*, 558−569.
(40) Laibinis, P. E.; Whitesides, G. M.; Allara, D. L.; Tao, Y. T.; Parikh, A. N.; Nuzzo, R. G. Comparison of the Structures and wetting properties of Self-Assembled Monolayers of *n*-Alkanethiols on the Coinage Metal Surfaces, Copper, Silver, and Gold. *J. Am. Chem. Soc.* **1991**, *113*, 7152−7167.
(41) Zenasni, O.; Marquez, M. D.; Jamison, A. C.; Lee, H. J.; Czader, A.; Lee, T. R. Inverted Surface Dipoles in Fluorinated Self-Assembled Monolayers. *Chem. Mater.* **2015**, *27*, 7433−7446.
(42) Baghbanzadeh, M.; Simeone, F. C.; Bowers, C. M.; Liao, K.-C.; Thuo, M.; Baghbanzadeh, M.; Miller, M. S.; Carmichael, T. B.; Whitesides, G. M. Odd−Even Effects in Charge Transport Across *n*-Alkanethiolate-Based SAMs. *J. Am. Chem. Soc.* **2014**, *136*, 16919−16925.
(43) Tao, F.; Bernasek, S. L. Understanding Odd−Even Effects in Organic Self-Assembled Monolayers. *Chem. Rev.* **2007**, *107*, 1408−1453.
(44) Park, J.-S.; Vo, A. N.; Barriet, D.; Shon, Y.-S.; Lee, T. R. Systematic Control of the Packing Density of Self-Assembled Monolayers Using Bidentate and Tridentate Chelating Alkanethiols. *Langmuir* **2005**, *21*, 2902−2911.
(45) Lees, W. J.; Whitesides, G. M. Equilibrium Constants for Thiol-Disulfide Interchange Reactions: A Coherent, Corrected Set. *J. Org. Chem.* **1993**, *58*, 642−647.

NOTE ADDED AFTER ASAP PUBLICATION

Due to a production error, this article published inadvertently September 1, 2020. The corrected article published September 2, 2020.

https://dx.doi.org/10.1021/acs.langmuir.0c01373
Langmuir 2020, 36, 10699−10707